Review on spontaneous magnetic fields in laser-produced plasmas: Phenomena and measurements

By J. A. STAMPER

U.S. Naval Research Laboratory, Washington, D.C. 20375-5000

Large (megagauss) "spontaneous" magnetic fields are produced by laser–plasma interactions when a short, powerful laser pulse is focused to a small diameter onto a solid target. The relevance of these magnetic fields to inertial confinement fusion applications depends on the numerous ways in which they can affect laser–plasma interactions and the resulting plasma. Theoretical studies have dealt with a variety (thermal, radiative, and dynamo) of generation mechanisms and with the associated transport and instability phenomena. The fields, originally observed with small induction probes placed near the target, have been studied in the focal region by optical methods. These optical diagnostics have used Faraday rotation of a probing laser beam and Zeeman profiles of emitted spectral lines.

1. Introduction

In the study of the physics relevant to inertial confinement fusion (ICF) by lasers, a short, powerful pulse of laser radiation is focused to a small diameter onto a solid target. The resulting laser-produced plasma is observed to contain a large magnetic field, produced directly as a result of the laser–plasma interaction. This is the "spontaneous" or "self-generated" magnetic field, which is discussed here. A more descriptive term would be a laser-generated magnetic field, since they do not generally require an initial field but do require the laser–plasma interaction. The implied large magnetic field generation rate was, at first, quite surprising, but is, as we shall see, a direct consequence of the character of the focused laser pulse.

The earliest measurements were made with small induction probes placed near the target. The fields were first reported in the Russian literature—both for a gas breakdown (Korobkin & Serov 1966) and for a solid target (Askar'yan *et al.* 1967). Rather large fields (kilogauss) were reported later (Stamper *et al.* 1971) and explained in terms of thermal sources. It became apparent that very large fields (megagauss) could exist in the laser focal region and that they could affect the physics of ICF in a variety of ways. These megagauss fields were later measured with the use of Faraday rotation of a probing laser beam.

1.1 *Relation to laser pulse character*

The laser-produced plasma can be roughly represented, with its axis along the laser axis, by a cylinder of radius r (determined by laser focal radius) and thickness w. The laser-plasma interaction can then be modeled as an electric circuit (Tidman & Stamper 1973). One can write $V = IR + L(dI/dt)$, where the voltage V is energy per unit charge kT/e, the re-

sistance is $R = \rho w/\pi r^2$ (ρ is resistivity), and the inductance is $L = w/c^2$. The capacitive drop can be neglected. Further, the resistive drop for a hot plasma can be neglected, since $L(dI/dt)/IR \sim \pi r^2/c^2\rho\tau \gg 1$, where τ is the laser pulse width. Basically, then, because of the small radius, the high temperature, and the short pulse width, the reactance is inductive. This is the reason for the large magnetic field generation. We have $dI/dt \sim kT/eL \sim c^2kT/ew$, and, when we use Ampere's law, $B = 2I/rc$ gives

$$\frac{dB}{dt} \sim \frac{2c}{e}\frac{kT}{rw}. \tag{1}$$

Thus the high-intensity (large-kT), short pulse onto a solid target (small w), when tightly focused (small r), produces a very large field generation rate. The generation rate given by equation (1) agrees (within a factor of 2) with that derived from the thermal source term discussed in Section 2.1.

1.2 *Relevance to inertial confinement fusion*

Most experiments and many of the numerical studies have been for a single laser beam focused onto a planar target. However, in ICF applications, multiple beams are focused as uniformly as possible onto a spherical pellet. Hopefully, with reasonably uniform illumination to minimize tangential gradients, the magnetic complications are minimized. Nevertheless, there is reason to be cautious. Nuckolls (1973) indicated that a 5% laser intensity variation, with 1-micron laser light, could reduce the yield by an order of magnitude if classical transport is valid. The earlier pellet designs, requiring higher laser intensities, were less forgiving for nonuniformities of laser radiation in the lower-density regions ($\sim 10^{20}$–10^{21} cm^{-3}) where absorption occurred. At higher laser intensities ($\geq 10^{15}$ W/cm^2), where the direct effects of laser radiation are important, field generation also depends on the laser polarization (resonant absorption) and the local direction of the Poynting flux (field momentum deposition). A radial direction for the laser energy flux would be required—in addition to the laser intensity magnitude's being uniform over the pellet surface. The fields can also grow from small initial perturbations in the temperature or density via field-generating instabilities (Section 3.3).

The magnetic fields can affect pellet performance in several ways. The greatest initial concern was that pellet performance would be degraded owing to reduce thermal transport (Section 3.1) and its effect on implosion symmetry (Nuckolls 1973). This was due to the magnetic fields generated in the lower-density absorption region by nonuniform laser irradiation. There were also early studies (i.e., Tidman 1975) of the large magnetic fields generated in the dense, imploding target material, exacerbated by composition discontinuities and shocks. Later studies of the magnetic fields generated in the ablation region and associated with the Rayleigh–Taylor (R–T) instability (Sections 2.3 and 3.4) raised the concern of inhibited thermal flux from the absorption to the ablation region and a consequent decrease in ablation pressure. The magnetic fields can also have a beneficial effect. Resonant absorption can be highly efficient in a magnetized plasma (Woo, Estabrook & DeGroot 1978). The magnetic fields can be convected toward the ablation region and amplified (Nishiguchi *et al.* 1984). In the overdense region these fields could inhibit hot-electron preheat of the fuel. The fields, if large enough, could reduce the R–T growth rate (Section 2.3). The magnetic fields, amplified in the fuel by plasma compression, could greatly increase the yield (Jones & Mead 1986). The challenge is to understand and to represent the complex magnetic contributions (Sections 2 and 3) with sufficient accuracy to predict actual pellet performance.

The magnetic field effects that have been discussed refer to the magnetic fields that would develop for conventional laser-driven ICF. However, it may be possible to employ the magnetic fields in a nonconventional approach. One approach (Hauer & Mason 1983; Daido *et al.* 1986) uses the high-intensity irradiation of nearby structures to produce large currents and magnetic fields. Another approach (Hasegawa *et al.* 1986) is to irradiate (through a hole) the inside of a spherical metallic shell and to utilize the thermal insulation of the magnetic fields, spread by the $\mathbf{E} \times \mathbf{B}$ drift (Section 3.2), over the inner surface.

2. Theoretical background

2.1 *Generation of magnetic fields*

The basic equation describing the development of the slowly varying magnetic field is dependent, through Faraday's law, on the electric field in a laser-produced plasma. The electric field is evaluated here from a laminar fluid electron equation of motion:

$$nm \frac{d\mathbf{V}_e}{dt} = -ne\left(\mathbf{E} + \frac{1}{c}\,\mathbf{V}_e \times \mathbf{B}\right) - \nabla\cdot\mathbf{P}_e + \mathbf{f}^c + \mathbf{f}^r. \tag{2}$$

Owing to the small electron inertia, various forces acting on the electron fluid tend to be balanced with the electrical force $-ne\mathbf{E}$, where e is the magnitude of the electronic change. The collisional force $\mathbf{f}^c$ is ne times the sum of the resistive drag ($\mathbf{J}^o/\sigma$) and thermal ($\alpha\nabla T$) forces. A constant scalar plasma conductivity σ and thermoelectric power α are assumed in this subsection. The radiative force $\mathbf{f}^r$ and the current density $\mathbf{J}^r$ (used in Ampere's law) are due directly to time correlations in the high-frequency quantities associated with the electromagnetic field of the laser radiation. The total radiative force $\mathbf{f}^r$ is the sum of the radiative Hall force $\mathbf{J}^r \times \mathbf{B}/c$ and the (initially) zero magnetic field radiative force $\mathbf{f}_0^r$. The radiative effects are discussed in detail in Section 4.

Electron inertia effects are ignored here but are discussed in Section 2.2. Taking the curl of equation (2), where Faraday's law $c\nabla \times \mathbf{E} = -\partial\mathbf{B}/\partial t$ and Ampere's law $c\nabla \times \mathbf{B} = 4\pi(\mathbf{J}^o + \mathbf{J}^r) + \partial\mathbf{E}/\partial t$ are used, gives

$$\frac{\partial\mathbf{B}}{\partial t} = \nabla \times (\mathbf{V} \times \mathbf{B}) + \frac{c^2}{4\pi\sigma}\,\nabla^2\mathbf{B} - \nabla \times \left[\left(\frac{\mathbf{J}^0 + \mathbf{J}^r}{ne}\right) \times \mathbf{B}\right] + \mathbf{S}. \tag{3}$$

This is the equation describing the development of the magnetic field. The first term on the right-hand side describes convection of the magnetic field with the plasma and can result in the conversion of plasma flow energy into magnetic field energy (dynamo effect, discussed in Section 3.5). The second term describes diffusion of the magnetic field with respect to the plasma, or conversion of magnetic field energy to thermal energy; $c^2/4\pi\sigma$ is magnetic diffusivity. The third term describes the redistribution of the magnetic field due to the collisionless Hall forces associated with the ordinary ($\mathbf{J}^o$) and radiative ($\mathbf{J}^r$) currents. Note that $\mathbf{V}_e = \mathbf{V} - \mathbf{J}^o/ne$, where $\mathbf{V}_e$ and $\mathbf{V}$ are electron and plasma velocities, respectively. The last term $\mathbf{S}$ is the magnetic source term, describing magnetic field generation. It can be expressed as $-c\nabla \times (\mathbf{E}^o + \mathbf{E}^r)$, where $\mathbf{E}^r = \mathbf{f}_0^r/ne - \mathbf{J}^r/\sigma$ (for scalar conductivity σ) is the radiative field and

$$\mathbf{E}^o = -\frac{1}{ne}\,\nabla\cdot\mathbf{P}_e + \alpha\nabla T. \tag{4}$$

These terms, due to the electron pressure and the thermal force, are responsible for the thermal source term $\mathbf{S}'$. The radiative source term $\mathbf{S}^r = -c\nabla \times \mathbf{E}^r$ is discussed in Section 4. Other source terms are present when a kinetic, rather than a fluid, description is used (Haines 1986). For a turbulent plasma (Bychenkov, Gradov & Chokparova 1984), the turbulence affects not only the magnetic field generation but also the transport; e.g., the field diffusion is anisotropic.

The usually dominant term, leading to the well-known $\nabla T \times \nabla n$ source, is the one due to an isotropic pressure. Using $P_e = nkT$ in $\mathbf{S}' = -c\nabla \times \mathbf{E}^o$, where $\mathbf{E}^o = -(1/ne)\nabla P_e$ gives

$$\mathbf{S}' = \frac{ck}{ne}\,\nabla T \times \nabla n. \tag{5}$$

Although it was originally thought that thermal sources ($\mathbf{S}' \neq 0$) required the electrons to be nonadiabatic, it was pointed out by Widner & Wright (1974) that the adiabatic condition $[d(Tn^{1-\gamma})/dt = 0$, where $d/dt = \partial/\partial t + \mathbf{V}_e\cdot\nabla]$ does not imply, in a time-dependent problem, the vanishing ($\nabla T \| \nabla n$) of the thermal source term. This is due to the mixing of space and time variations in nonsteady flow. $\mathbf{S}'$ is in an azimuthal direction about a normally incident laser beam. For a right-handed cylindrical coordinate system (r,ϕ,z), ∇T is in the $-\hat{r}$ direction (toward the axis) and ∇n is in the $-\hat{z}$ direction (into the target), so that $\mathbf{S}'$ is the $-\hat{\phi}$ direction, corresponding to an axial electron flow out of the target.

Although it was assumed, in the thermal source term of equation (5), that electron pressure is a scalar, the general tensor character of electron pressure can be important in magnetic field generation. It was recognized (Stamper 1972) that a linearly polarized laser beam would produce, at high irradiance, enhanced heating along the laser electric field and that the resulting pressure anisotropy would generate a nonazimuthal magnetic field. Kinetic theory, with ponderomotive modifications (Shkarofsky 1980; Mora & Pellat 1981a), has provided a basis for radiation pressure effects (Section 4) as well as the laser-induced tensor character of the electron pressure.

The discussion of this section has been concerned with equation (3), which depends on a magnetic source term or magnetic field generation rate. It assumes that the laser–plasma interaction can be described in terms of forces acting on the electron fluid and is explicit in the time variation of the field. However, when the direct effects of laser radiation (Section 4) are important, there are situations where it is easier to describe current sources, such as the nonlinear current of resonant absorption (Section 4.3) or electron drifts due to laser field momentum (Section 4.4). One can then determine the spatial variation of the magnetic field directly from Ampere's law.

2.2 *Electron vorticity and magnetic fields*

The left-hand side of equation (2), where $d\mathbf{V}_e/dt = \partial\mathbf{V}_e/\partial t + \mathbf{V}_e\nabla\cdot\mathbf{V}_e$ is the convective derivative, is the inertial, or mass-dependent, force. On taking the curl of equation (2) and using the identity $\mathbf{V}_e\cdot\nabla\mathbf{V}_e \equiv \frac{1}{2}\nabla V_e^2 - \mathbf{V}_e \times (\nabla \times \mathbf{V}_e)$, one finds that $\nabla \times (d\mathbf{V}_e/dt)$ can be written in terms of the kinematic vorticity $\nabla \times V_e$ as $\partial(\nabla \times V_e)/\partial t - \nabla \times [V_e \times (\nabla \times V_e)]$. These two terms can be combined, respectively, with the electric (via Faraday's law) and magnetic parts of the Lorentz force to give $\partial\Omega_e'/\partial t - \nabla \times (\mathbf{V}_e \times \Omega_e')$, where Ω_e' is a generalized electron vorticity that is the sum of the kinematic vorticity $\Omega_e = \nabla \times \mathbf{V}_e$ and a magnetic vorticity $-e\mathbf{B}/mc$. Kinematic vorticity is the fluid circulation frequency and magnetic vorticity is the particle cyclotron frequency. Thus we could have retained electron inertia effects by taking the curl of equation (2) and writing the result in terms of the generalized vorticity rather than directly in terms of the magnetic field. In either case the thermal source term is a baroclinic source (proportional to $\nabla n \times \nabla P_e$).

Let us examine the conditions under which we can ignore electron inertia effects, or kinematic vorticity. Under most conditions the ions are relatively immobile and the electron velocity is proportional to the electric current density. Then Ampere's law shows that the ratio of kinematic vorticity ($\nabla \times \mathbf{V}_e$) to magnetic vorticity ($-e\mathbf{B}/m_e c$) is the square of the ratio of the collision-free spin depth (c/ω_{pe}) to the gradient scale length L of the magnetic fields. Since c/ω_{pe} is 0.5 microns at 10^{20} cm^{-3} ($0.1 n_{cr}$ for 1-micron laser light), the electron vorticity can be ignored in calculating the growth of multimicron scale length magnetic fields. However, Jones (1983) showed that electron inertia and vorticity cannot be ignored in surface waves associated with the magnetic field. This is discussed further in Section 3.2.

An equation for total ion vorticity (Hasegawa & Mima 1978) can be derived in a similar way. Taking the curl of the ion equation of motion and using Faraday's law shows that the total ion vorticity $\nabla \times \mathbf{V}_i + e\mathbf{B}/m_i c$ grows with the baroclinic source $(1/n^2 m_i)\nabla n \times \nabla P_i$, depending on ion pressure. Since the ion and plasma velocities are approximately the same, this appears to show that plasma vorticity and magnetic fields grow on an even footing. However, if $\partial \mathbf{B}/\partial t$ is substituted from the magnetic field equation, the thermal source term combines with the ion pressure source term, so that plasma kinematic vorticity responds, as expected, to the baroclinic source depending on total pressure — independently of magnetic fields. Thus, contrary to the situation with electrons, the concept of ion magnetic vorticity is not very useful for the thermal generation of magnetic fields.

Finite electron inertia effects have also been considered in a different context from electron vorticity. Haines (1986) included these terms in his magnetic field generation equation and noted their relevance to surface transport. Auluck (1986) gave arguments that the finite plasma frequency magnetohydrodynamic equations imply that large magnetic fields are spontaneously generated, even in a symmetric ICF explosion. Generally, one must consider electron inertia effects when there are spatial variations on the scale of the collision-free skin depth.

2.3 *Plasma vorticity and the Rayleigh–Taylor instability*

It is easy to see that vorticity is basic to the R–T instability. Consider a fluid interface (heavy fluid on top) in a gravitational field. An interface perturbation has heavy fluid extending into the troughs and light fluid extending into the crests. Because of the slope at the midpoint, there is a gravity component along the interface. The resulting differential acceleration drives a velocity shear or vorticity, with more heavy fluid sliding into the troughs and more light fluid rising into the crests. This increases the perturbation amplitude and slope.

A two-fluid description can be used to analyze the simultaneous growth of magnetic fields and the R–T instability. As noted by Spitzer (1962), it is less cumbersome in the more general case, where both hydrodynamic and electromagnetic effects are important, to use the plasma velocity $\mathbf{V} = (n_i m_i \mathbf{V}_i + n_e m_e \mathbf{V}_e)/\rho$, where $\rho = n_i m_i + n_e m_e$, and the electric current density $\mathbf{J} = e(n_i \mathbf{V}_i - n_e \mathbf{V}_e)$ instead of the ion ($\mathbf{V}_i$) and electron ($\mathbf{V}_e$) fluid velocities. Taking the curl of the equation for $\partial \mathbf{J}/\partial t$ (generalized Ohm's law), using Faraday's law, and ignoring electron inertia and terms of order m_e/m_i gives our equation for the magnetic field evolution with the thermal source term $\mathbf{S} = -(c/n_e^2 e)\nabla n_e \times \nabla P_e$. Note that the magnetic source term depends on electron pressure. Taking the curl of the linearized equation for $\partial \mathbf{V}/\partial t$ (equation of motion), in an accelerated frame with effective gravity $\mathbf{g}$, gives the equation for plasma vorticity $\mathbf{\Omega} = \nabla \times \mathbf{V}$ evolution,

$$\frac{\partial \mathbf{\Omega}}{\partial t} = \frac{1}{c} \, \nabla \times \left(\frac{1}{\rho} \, \mathbf{J} \times \mathbf{B} \right) - \nabla \times \left(\frac{1}{\rho} \, \nabla P \right), \tag{6}$$

where we assume that $\nabla \times \mathbf{g}$ is small. If $n_e = n_i = n$, then the source term for vorticity is $(1/n^2 m_i)\nabla n \times \nabla P$, where P is total $(P_e + P_i)$ pressure. When the $\mathbf{J} \times \mathbf{B}$ force can be neglected, differentiating equation (6) and using the equation of motion shows that, for small perturbations, $\partial^2 \Omega/\partial t^2$ can be expressed as $\mathbf{g} \times (\nabla \times \Omega)$. For growing modes this gives the classical growth rate $\sqrt{kg}$ for the R–T instability.

One should note a particular consequence of the absence (for a neutral plasma) of the electric field from the plasma equation of motion. The plasma kinematic vorticity (in contrast with the electron and ion fluid cases) does not have a magnetic analog. Although the plasma kinematic vorticity is basic to the R–T instability, the accompanying magnetic field generation is not basic to the R–T instability but is rather a consequence of the response of the electron density and temperature gradients to plasma dynamics. However, magnetic field generation is expected, since, owing to their small inertia, electrons respond quickly to plasma gradients.

If the magnetic fields are larger enough, the magnetic stress can affect the growth of the R–T instability. Since the magnetic stress along a field line is a tension, the magnetic field acts for $\mathbf{k} \| \mathbf{B}$ (in analogy with surface tension) as a stabilizing effect. According to Chandrasekhar (1961), γ^2/kg (where γ is R–T growth rate) is given for $\mathbf{B} \perp \mathbf{g}$ by $(\rho_2 - \rho_1)/(\rho_2 + \rho_1)$ minus a (stabilizing) term W_b/W_g, where $W_b = B^2/8\pi$ and $W_g = \bar{\rho}g/k^*$, with $\bar{\rho} = (\rho_1 + \rho_2)/2$ and $k^* = (\mathbf{k}\cdot\mathbf{B})^2/kB^2$. Since the thermally generated magnetic fields would initially be nearly normal to $\mathbf{k}$, k^*/k would initially be small. However (see Section 2.4), as the fields grow to where $\omega_c \tau$ is not small compared with unity, the various magnetic field effects on transport phenomena increase the size of k^*/k and thus the magnetic stabilization.

2.4 *Magnetic field effects on transport phenomena*

We consider briefly in this section (in contrast with the fluid theory of Section 2.1) some results of a kinetic description (Braginskii 1965) that includes the tensor character of the transport coefficients. It is useful, in a discussion of transport phenomena, to show the effect of an electric current density $\mathbf{J}$ and temperature gradient ∇T on the collisional electric field $\mathbf{E}^*$ and the thermal energy flux $\mathbf{q}$. This electric field can be expressed as $\boldsymbol{\rho} \cdot \mathbf{J} + \boldsymbol{\alpha} \cdot \nabla T$, where the transport coefficients are electric resistivity ρ and thermoelectric power α. Similarly, the heat flux can be expressed as $-\boldsymbol{\kappa} \cdot \nabla T + T\boldsymbol{\alpha} \cdot \mathbf{J}$, where the coefficient κ is thermal conductivity. The components of these transport coefficients depend implicitly in the magnetic field through the Hall parameter $\omega_c \tau$, which occurs in the transport integrals (over the velocity distribution). $\omega_c \tau$ is the number of electron cyclotron gyrations between collisions. For example, the ratio $\kappa_\perp/\kappa_\|$ of the perpendicular to parallel (to $\mathbf{B}$) components of κ is, for large $\omega_c \tau$, of the order of $1/(1 + \omega_c^2\tau^2)$. For quantitative calculations one should use the improved transport coefficients (Epperlein & Haines 1986) obtained by a numerical solution of the Fokker–Planck equation.

The magnetic field also produces, through the Lorentz force, skew-symmetric (off-diagonal) components in the transport coefficients. There is thus an explicit dependence on the magnetic field in the form of a cross product with the field. These skew-symmetric (denoted by subscript $\wedge$) contributions to the collisional field and the heat flux can be expressed as

$$\mathbf{E}_\wedge^* = \underset{\text{(Hall effect)}}{R\mathbf{B} \times \mathbf{J}} - \underset{\text{(Nernst effect)}}{Q\mathbf{B} \times \nabla T}, \tag{7}$$

$$\mathbf{q}_\wedge = \underset{\text{(Ettinghausen effect)}}{-TQ\mathbf{B} \times \mathbf{J}} + \underset{\text{(Righi–Leduc effect)}}{S\kappa_\wedge \mathbf{B} \times \nabla T}, \tag{8}$$

where R is the Hall coefficient, Q is the Nernst coefficient, $\kappa_\wedge$ is cross-thermal conductivity, and S is the Righi–Leduc coefficient. For the convenience of discussion, the names (from solid-state physics) of various effects have been noted under each term. Note that the Nernst coefficient Q also occurs in the Ettinghausen effect. This is due to the Onsager reciprocity relations (DeGroot 1952) between certain transport coefficients.

For example, we can see the effect ($\nabla \times \mathbf{E}_\wedge^*$) of the collisional field on magnetic field generation. The Hall effect produces magnetic field contributions normal to those already present and is important in the spatial distribution of the fields. The Nernst effect can produce a magnetic field in the same direction as the original field and thus lead to an instability. Similarly, the skew-symmetric contributions to the heat flux can be important. The Ettinghausen effect contributes to heat flux both along the field and along the gradient. The Righi–Leduc effect produces heat flux perpendicular to both the magnetic field and the gradient. It contributes to cross-field heat flux and can lead to instabilities.

In the hotter and less dense critical region, $\omega_c \tau$ can be very large and thus can significantly reduce the lateral heat flux. In the cooler and denser ablation region, $\omega_c \tau$ may have a maximum of the order of unity. However, the skew-symmetric effects maximize for $\omega_c \tau$ around 1 and so could be important in the ablation region. For example, it may be necessary to include these effects in simulating the R–T instability.

3. Studies of magnetic fields and related phenomena

3.1 *Thermal transport effects*

Thermal transport can be affected by the magnetic field in several ways, including implicit dependence on the magnetic field through the Hall parameter ($\omega_c \tau$), explicit dependence through the skew-symmetric contributions (Section 2.4), and magnetic turbulence effects. Some examples are cross-field thermal inhibition [$\kappa_\perp/\kappa_\parallel \sim 1/(1 + \omega_c^2 \tau^2)$], magnetic redirection of conducted heat flux (Righi–Leduc effect), magnetic redirection of convected heat flux (Nernst–Ettinghausen effect), and Nernst convection of the magnetic field.

Thermal transport inhibition due to magnetic fields is necessary to explain X-ray emission from laser-produced plasmas. Two-dimensional simulations, including the magnetic fields, were necessary to account for both the X-ray conversion efficiency (Winsor & Tidman 1973; Colombant *et al.* 1975) and the absolute X-ray spectra (Ripin *et al.* 1975; Mead *et al.* 1976). Inhibited thermal flux is also evident from ICF studies. An early two-dimensional simulation of an experiment on deuterium plasmas (Chase, LeBlanc & Wilson 1973) showed that including the magnetic field gave a better agreement with experiment. Reduced implosion velocities (Attwood 1978) and reduced classical absorption (Mead *et al.* 1978) are two signatures of the flux inhibition. The magnetic fields for this thermal flux inhibition could come from the various generation mechanisms (Sections 2.1 and 4.2) operative in the lower-density laser absorption region. However, large magnetic fields generated in the ablation region on account of laser nonuniformities (Emery 1984) or the R–T instability (Section 3.4) are convected to the lower-density regions.

Turbulence or stochastic processes can also play an important role in transport effects. Ion-acoustic turbulence has itself been considered (Manheimer 1977) as a candidate for thermal flux inhibition. However, ion-acoustic turbulence can be important in magnetic field generation (Bychenkov, Gradov & Chokparova 1984). These authors also point out the importance of anisotropy of magnetic field diffusion for turbulent plasmas. Whenever magnetic fields have a small-scale, disordered structure, there is enhanced transport across the magnetic field (Max, Manheimer & Thomson 1978). The energy and the direction of superthermal electrons, stochastically accelerated by electrostatic turbulence, can be strongly affected by the magnetic fields (Tidman & Stamper 1973).

There has been considerable interest in the effect of the Nernst field $\mathbf{E}_N = -Q\mathbf{B} \times \nabla T$ (see Section 2.4) on transport phenomena. The Nernst contribution ($\mathbf{S}_N = -c\nabla \times \mathbf{E}_N$) to the magnetic field growth $\partial\mathbf{B}/\partial t$ can be viewed either as a convection or as a source of the magnetic field. Nernst convection of the magnetic field with the heat flux is important in the overdense plasma ($\omega_c\tau \ll 1$) and has been considered by Bol'shov, Dreizin & Dykhne (1974), Bol'shov *et al.* (1979), and Nishiguchi *et al.* (1984). One can express $\mathbf{S}_N$ as $\nabla \times (\mathbf{V}_N \times \mathbf{B})$, where the Nernst convection velocity $\mathbf{V}_N$ is $-cQ\nabla T$. Since $Q > 0$, the magnetic field is convected toward colder regions. Physically, the magnetic field is convected with the heat flux, since, owing to the velocity dependence of collision frequency, the magnetic field is primarily frozen to the warm electrons, responsible for heat flux. Nishiguchi *et al.* found, from analytic and numerical studies, that $\mathbf{B}$ is convected toward the overdense region and amplified by a factor of 10–100. The amplified fields could reduce preheat and increase hydrodynamic coupling. Numerical simulations in the underdense plasma ($\omega_c\tau \gg 1$) (Colombant & Winsor 1977) show that the Nernst effect shifts the magnetic fields to larger radii and later times. Since $cQ\mathbf{B}\nabla^2 T$ is a dominant contribution to $\mathbf{S}_N$, the sign of $\mathbf{S}_N\cdot\mathbf{B}$ is that of $\nabla^2 T$. Thus the fields are enhanced at radii greater than that of the temperature inflection point and are reduced at smaller radii.

3.2 *Surface transport phenomena*

Numerical simulations by Forslund & Brackbill (1982) provided an explanation for a puzzling phenomenon observed in high-irradiance CO_2 experiments. This was the rapid convection of laser energy across the target surface, coupled with inhibited electron transport and fast ion loss (Yates *et al.* 1982; Kieffer *et al.* 1983; Terai *et al.* 1985). Forslund and Brackbill found that the thermally generated magnetic field was convected radially outward with energetic electrons that were subject to an $\mathbf{E} \times \mathbf{B}$ drift along the surface. The azimuthal ($\nabla T \times \nabla n$) magnetic field is right handed about an axis (conventional current) into the target. The ambipolar electric field is directed from the ions to the more mobile electrons, or outward. The $\mathbf{E} \times \mathbf{B}$ drift is thus radially outward from the laser axis.

A basis for insight into this phenomenon had been given earlier by Pert (1977). He described "thermal magnetic" waves that propagated along surfaces of constant density and noted that, in a severely flux-limited plasma, the waves may represent a significant contribution to energy transport. For the analysis the field-to-particle energy conversion can be represented, under adiabatic conditions, as compressional heating $d\epsilon/dt = -P_e\nabla \cdot \mathbf{V}_e$, where $\epsilon = (3/2)nkT_e$ is internal energy density. Charge conservation $[\nabla \cdot (n\mathbf{V}_e) = 0]$ for a neutral plasma implies that this heating is the heating $\mathbf{E}_0\cdot\mathbf{J}$ due to current oscillations along the density contribution $\mathbf{E}_0 = -(kT/e)\nabla \ln n$ to the ambipolar field. Ampere's law is then used to relate $\mathbf{J}$ to the magnetic field. Pert represented the particle-to-field energy conversion $\partial\mathbf{B}/\partial t$ by the thermal source term [equation (5)]. However, Jones (1983) pointed out that, for surface waves or, for that matter, any phenomenon with a spatial scale not large compared with c/ω_{pe}, one must include electron inertia or vorticity effects in the field generation description (see Section 2.2). The analysis of Jones, correctly including electron vorticity, shows that there is a new class of thermal magnetic surface waves that can exist in discrete modes resembling waveguide modes.

3.3 *Field-generating instabilities*

Under the rich variety of conditions that can exist, subject to the various thermomagnetic phenomena, there are some that can lead to an unstable growth of magnetic fields. One of the earliest and most considered is now called the thermomagnetic instability (Tidman & Shanny 1974; Alterkop & Mishin 1974; Alterkop, Mishin & Rukhadze 1974; Bol'shov,

Dreizin & Dykhne 1974). These studies involved the Righi–Leduc or cross-field heat flux $\mathbf{q}_\wedge = S\kappa_\wedge \, \mathbf{B} \times \nabla T$, where $\kappa_\wedge > 0$. Assume that ∇T and ∇n are initially parallel, so that the thermal source vanishes, and introduce a small perturbation $\nabla_\perp T$ normal to ∇n. The thermally generated field then gives a cross-field heat flux along $(\nabla T \cdot \nabla n) \nabla_\perp T$, so that for $\nabla T \cdot \nabla n > 0$ the perturbation is enhanced. Whether an exponential growth occurs depends on other conditions. Bol'shov, Dreizin & Dykhne (1974) and Bol'shov *et al.* (1979) pointed out the stabilizing influence of Nernst convection (Section 3.1) of the fields out of the generation region. Brownell (1979) also included field diffusion and found a critical wavelength, below which field diffusion smears out the growth. The instability can occur only at high temperature.

An instability described by Haines (1981) occurs in the dense, cold plasma near the ablation surface. This is the thermal instability, in which a large heat flow is represented as a flow of hot, collisionless electrons that are balanced ($\mathbf{J}_c + \mathbf{J}_h = \mathbf{0}$) by an oppositely directed current of cold, collisional electrons. A local increase in the electron temperature increases the cold return current ($\sigma \propto T_e^{3/2}$), which, via Joule heating, further increases the electron temperature. Because of the short wavelength and the fast growth, this instability has been proposed to explain the fine-scale structure observed by Willi, Rumsby & Duncan (1981). The magnetic source for the thermal instability arises from the counterstreaming electrons and is reminiscent of the Weibel instability, which depends on an anisotropy in the electron velocity distribution. Numerical simulations of the anisotropic heating resulting from resonant absorption (Estabrook 1981) showed a Weibel-like instability in which fine-scale magnetic fields in the megagauss range were produced.

3.4 *Rayleigh–Taylor instability*

The R–T instability, in the ablation region of an imploding ICF pellet, is a major concern. Without stabilizing effects, the R–T growth of density and pressure structures for high-aspect-ratio pellets would seriously degrade the implosion symmetry. A background discussion of the R–T instability and its association with the magnetic fields was given in Section 2.

Simulations and analytic estimates (Yabe & Niu 1976; Afanasév *et al.* 1978; Mima, Tajima & Leboeuf 1978; Emery 1984; Nishiguchi & Yabe 1983) of the magnetic fields associated with the R–T instability show that they can be in the megagauss range. These fields could affect the pellet performance in several ways. Reduction of the thermal flux from the critical region to the ablation region reduces the ablation pressure. The largest fields could affect the dynamics and even the R–T growth (Section 2.3).

Yabe & Niu (1976) noted that the thermal source for magnetic fields does exist, since the pressure perturbation due to convection cannot compensate that due to a gravity component along the interface. Their simulations showed fields in the megagauss range. Afanasév *et al.* (1978) considered the R–T magnetic fields generated in a narrow zone (few microns) near the front of the thermal wave in a spherical target and found that fields in the megagauss range were produced and were convected to a much larger, lower-density region. The R–T simulations of Mima, Tajima & Leboeuf (1978) also produced megagauss fields but *did not include resistive diffusion*. They noted that turbulent magnetic fields ahead of the ablation layer should lower the hot-electron flux from the corona and thus reduce core preheat.

The magnetic fields generated during the R–T instability can also have a feedback effect on the instability. Nishiguchi & Yabe (1983) pointed out that the magnetic fields give a nonconventional character to the instability. The magnetically inhibited heat flux changes the mode structure by a heat flux filamentation through the magnetic neutral sheet and mod-

ifies the zero-order structure of the ablation front. Evans (1986), using the ratio of the magnetic to fluid vorticity energy density, estimated that the magnetic fields can affect the R–T growth rate only for large k (wavelength less than a few microns). As it was noted in Section 2.3 (Chandresekhar 1961), the magnetic field can have a stabilizing effect.

3.5 *The Dynamo effect*

The term "magnetic field generation" has been used thus far to mean the generation of magnetic field energy from sources that are independent of the magnetic field. However, when a magnetic field already exists, further magnetic field energy can be generated from the directed energy of plasma flow. This is called the dynamo effect and is represented by the first term $[\nabla \times (V \times B)]$ on the right-hand side of equation (3). The initial (seed) magnetic field can be generated from one of the other sources (thermal or radiative) that have been discussed. The term $\nabla \times (V \times B)$ also represents convection of the magnetic field with the plasma and so represents both the dynamo effect and the redistribution of the magnetic field with plasma flow. An early discussion of these effects in laser-produced plasmas (Witalis 1973) pointed out that the dynamo effect required complicated plasma motions. Motions such as nonuniform rotation and turbulent and cyclonic convection can account for the magnetic fields in stars and galaxies.

Experimental studies concerning the dynamo effect have been based on the observation of axial magnetic fields (Briand *et al.* 1985) and of small-scale plasma structure (Yabe *et al.* 1983; Kitagawa *et al.* 1986), along with a theoretical model to show how, through plasma flow, a large-scale magnetic field is produced. However, the theoretical models of these studies were criticized by Dragila (1987) as misinterpreting dynamo action. He argued that these models actually represent a plasma flow redistribution of magnetic fields rather than dynamo generation of the fields. Dragila pointed out that a hydrodynamic dynamo must have both poloidal-to-toroidal and toroidal-to-poloidal producing mechanisms. Plasma turbulence is described as fitting these requirements, and an estimate is made of the fields generated by ion-acoustic turbulence in a laser-produced plasma. Axial fields in the megagauss range are predicted. It is interesting that ion-acoustic turbulence can generate large magnetic fields through either thermal sources (Bychenkov, Gradov & Chokparova 1984) or dynamo action (Dragila 1987).

It should be noted that an axial magnetic field, even at normal laser incidence, is not necessarily evidence for the dynamo effect. For a linearly polarized laser beam the preferential heating along the laser electric field produces an electron pressure anisotropy of the order of the ratio of radiation to thermal pressure. The magnetic fields for a high-irradiance experiment could have, by this mechanism, an appreciable axial component.

4. Direct effects of laser radiation

4.1 *Background discussion*

One of the more interesting physics areas for laser-produced plasmas is that of the direct effects of the high-frequency laser radiation. The radiative effects tend to be important at high laser irradiance ($\geq 10^{14}$ W/cm^2 for a Nd–glass laser), where the quiver velocity ($-e\omega\tilde{E}/mc$) is not small compared with the electron thermal velocity. Here, the quantities of interest on the usual (slow) time scale are due to time correlations in the products of two high-frequency quantities (denoted by a tilde), including the laser electromagnetic fields ($\tilde{E}, \tilde{B}$) and the density ($\tilde{n}$) and velocity ($\tilde{V}_e$) oscillations that they induce in the plasma. The correlations result from phase-shifting mechanisms such as plasma inhomogeneity or dis-

sipation. These slowly varying products and the effects associated with them are referred to as nonlinear, ponderomotive, or radiative. A good description of nonlinear phenomena was given by Hora (1981).

One should note that the interest is matched with a challenge when considering the complicated situation of real laser fields and plasma interactions for an experiment or ICF application. Two simplified approaches are useful. One uses a plane wave interacting with a one-dimensional plasma so that a detailed physics study can be made of interacting fields and plasma. Another approach is to use a more realistic focal geometry and a simplified physics study of interacting radiation pressure and plasma.

The time-averaged $\langle\ \rangle$ products or nonlinear contributions that are of particular interest include ponderomotive pressure $P^r = \langle \tilde{E}^2 \rangle / 8\pi$, field momentum density $\mathbf{g} = \langle \tilde{\mathbf{E}} \times \tilde{\mathbf{B}} \rangle / 4\pi c$, nonlinear current density $\mathbf{J}^r = -e\langle \tilde{\mathbf{V}}_e \tilde{n} \rangle$, and radiation pressure

$$\mathbf{P}^r = \frac{1}{4\pi}\left(\frac{1}{2}\langle \tilde{E}^2 + \tilde{B}^2 \rangle \mathbf{I} - \langle \epsilon_r \tilde{\mathbf{E}}\tilde{\mathbf{E}} + \tilde{\mathbf{B}}\tilde{\mathbf{B}} \rangle\right). \tag{9}$$

This radiation pressure is the sum of the laser field pressure (negative of Maxwell stress) and the high-frequency (quiver) electron pressure $mn\langle \tilde{\mathbf{V}}_e \tilde{\mathbf{V}}_e \rangle$. For sinusoidal time variation ($\partial/\partial t \to i\omega$ in complex notation), the high-frequency dielectric function $\epsilon_r + i\epsilon_i$ is defined in terms of the high-frequency conductivity ($\tilde{\mathbf{J}} = \sigma\tilde{\mathbf{E}}$) by $\epsilon = 1 + i4\pi\sigma/\omega$ and includes displacement current effects. For an effective collision frequency ν ($\sigma = ne^2/m\nu$), we have $\epsilon_r = 1 - \omega_p^2/(\omega^2 + \nu^2)$ and $\epsilon_i = \nu\omega_p^2/\omega(\omega^2 + \nu^2)$.

The radiative force density on the electrons is the sum of the collisionless Hall force $(1/c)\mathbf{J}^r \times \mathbf{B}$ and a radiative force $\mathbf{f}_0^r$ that is (initially) independent of the steady magnetic field. This force, which can be written as

$$\mathbf{f}_0^r = (\epsilon_r - 1)\nabla P^r + \epsilon_i \omega \mathbf{g} + \epsilon_r (m\nu/e)\mathbf{J}^r, \tag{10}$$

includes momentum transfer by radiation pressure variations ($-\nabla \cdot \mathbf{P}^r$) and collisions with ions ($-m\nu\langle \tilde{n}\tilde{\mathbf{V}}_e \rangle$). The first two terms on the right-hand side are due to radiation pressure, but the last term includes both radiation pressure and ion-collision effects.

The first term on the right-hand side of equation (10) is the ordinary ponderomotive force, which, through density profile modifications, can have an appreciable affect on laser–plasma interactions. The second term represents the force on the electrons due to field momentum deposition during absorption (Stamper 1976; Schmidt 1979). It is in the direction of the Poynting flux $\mathbf{I} = c^2\mathbf{g}$ and can be expressed as $KI\bar{n}/c$, where, for inverse bremsstrahlung, the absorption coefficient K is given by $\bar{n}[1 + (\nu/\omega)^2]K = (\omega_p/\omega)^2(\nu/c)$ and $\bar{n} = \sqrt{\epsilon_r}$ is the refractive index. The last term is the effective (from both radiation pressure and ion collisions) resistive drag due to the nonlinear current $\mathbf{J}^r$. Contributions to the nonlinear current are particularly important for resonant absorption, discussed in Section 4.3.

There is also a ponderomotive modification to the tensor electron pressure (Shkarofsky 1980; Mora & Pellat 1981a). The time-averaged electron distribution function becomes anisotropic. This could be included in the radiative force, but it is not considered here.

Once a steady magnetic field has been produced, there are radiative forces, such as the collisionless Hall force due to the nonlinear current, that depend on the magnetic field. The steady magnetic field is also a mechanism for producing phase shifts that directly result in a radiative force (Stamper & Bodner 1976). For a linearly polarized laser beam this magnetic radiative force is along (one direction of) the oscillating electric field.

Much of the background discussion in this section is based on a fluid description of the electrons. It has been recognized that, in a general analysis of magnetic field generation, a kinetic theory with ponderomotive modifications is needed. Bezzerides *et al.* (1977) used

a collision-free theory in the resonant absorption problem. Shkarofsky (1980) used a collisional kinetic theory with an arbitrary form for the time-averaged part of the velocity distribution. Anisotropy of this distribution was shown. Ponderomotive contributions were given for the (zero dc magnetic field) transport coefficients and collisional momentum transfer. Mora & Pellat (1979) described ponderomotive modifications in three regimes: collisionless, intermediate, and collisional. The results were applied in the collisionless regime to resonant absorption. These authors also (1981a) provided a general description of ponderomotive effects in magnetic field generation in the underdense plasma. They showed that, in addition to radiation pressure, there are ponderomotive modifications (laser-induced anisotropy) to the electron pressure. Mora & Pellat (1981b) also calculated magnetic field generation due to short-wavelength ion turbulence, using the Dawson and Öberman model. It should be noted that corrections have also been made (Epperlein & Haines 1986) to the transport coefficients usually used (Braginskii 1965) in collisional, magnetized plasma transport.

Magnetic fields due directly to circularly polarized laser radiation form a special case that is mentioned here only because it is essentially different from the other effects of this section and that is important only for extremely high ($\gtrsim 10^{17}$-W/cm^2) laser intensities. These magnetic fields are produced by the inverse Faraday effect (Steiger & Woods 1972). They are a result of plasma magnetization due to the magnetic moments of electrons in circular motion.

4.2 *Radiative magnetic field generation*

Dissipation ($\epsilon_i \neq 0$) is the primary mechanism that results in radiative forces that generate magnetic fields. The first discussion of magnetic field generation by a radiative mechanism (absorption) was given by Askar'yan *et al.* (1967). The role of dissipation in magnetic field generation became clear from the early calculations (Stamper & Tidman 1973; Thomson, Max & Estabrook 1975) utilizing the tensor character of radiation pressure. Although the role of field momentum deposition had been pointed out and resonant absorption had been studied (Thomson, Max & Estabrook 1975), it was not until the nonlinear current was explicitly included (Bezzerides *et al.* 1977) that rapid progress was made in the resonant absorption problem (discussed in Section 4.3).

One must mathematically represent the solenoidal nature of the radiative or ponderomotive forces in order to show magnetic field generation. In certain areas approximate treatments can completely misrepresent this solenoidal nature. An adiabatic treatment of the radiative force due to refraction shows a solenoidal nature with any realistic focal geometry. This follows since, in the adiabatic approximation, the radiation pressure for a dissipationless plasma (a real dielectric function $\epsilon = \bar{n}^2$) has the anisotropic form [$I(1 - \epsilon)/2\bar{n}c)\mathbf{l} + \mathbf{v}_g\mathbf{g}$, where $\mathbf{v}_g$ is group velocity. However, the general treatment shows that the refractive force is contained in the ordinary ponderomotive force [first term on the right-hand side of equation (3.10)] and is thus irrotational (Stamper 1977). The earlier argument by Stamper (1972) that an anisotropy of radiation pressure implied magnetic field generation was erroneous, since the adiabatically approximated radiation pressure was used. The fact that refraction does not generate magnetic fields is in keeping with our understanding of the role of dissipation.

From Section 2.1 the radiative part of the magnetic source term is

$$\mathbf{S}^r = -c\nabla \times (\mathbf{f}_0^r/ne - \mathbf{J}^r/\sigma). \tag{11}$$

The ordinary ponderomotive force ($\epsilon - 1)\nabla P^r$ does not generate magnetic fields, since the ponderomotive field ($\epsilon - 1)(\nabla P^r)/ne$ is irrotational. However, the field momentum de-

position and resistive drag forces both explicitly include dissipation ($\epsilon_i, \nu \neq 0$) and can thus generate magnetic fields.

One can consider a saturated magnetic field ($S^r = 0$), due solely to radiative effects. Then Ampere's law can be used (Bezzerides *et al.* 1977; Woo & DeGroot 1978b) to calculate the steady-state magnetic field. However, it should be recognized that, in an actual situation, the magnetic field may represent a balance between radiative field generation and nonradiative effects, such as convection or ordinary resistive diffusion.

Let us now evaluate, for later use, the magnetic source $\mathbf{S}_g^r$ due to field momentum deposition. The field $\epsilon_i \omega \mathbf{g}/ne$ has the same magnitude as the "nonpotential" (electric) field discussed by Askar'yan *et al.* (1967). This source term can be expressed simply in terms of the Poynting flux $\mathbf{I}$. Since $\epsilon_i \omega \mathbf{g}$ can be expressed (when $\nu \ll \omega$) as $n\nu \mathbf{I}/n_{cr}c^2$, we can write the source term as

$$\mathbf{S}_g^r = -J_c^{-1}\nabla \times (\nu \mathbf{I}), \tag{12}$$

where $J_c = n_{cr}ec = 1.45 \times 10^{22}$ esu for a Nd–glass laser ($n_{cr} = 10^{21}$ cm^{-3}).

One could also formally combine the terms depending on $\mathbf{J}^r$ in equation (11) to obtain a radiative source, similar to equation (12), showing how the nonlinear current with dissipation ($\nu \neq 0$) generates magnetic fields. This source term $(mc^2/eJ_c)\nabla \times (\nu \mathbf{J}^r)$, however, may not be so useful for calculations, since, unlike the irradiance or Poynting flux, $\mathbf{J}^r$ is not known from experimental conditions.

4.3 *Resonant absorption*

Magnetic fields are important in resonant absorption for two reasons: First, magnetic fields are produced in ordinary resonant absorption; second, there is a type of resonant absorption dependent on a magnetic field. Consider an electromagnetic wave incident at some angle θ to the density gradient and polarized perpendicularly to a steady magnetic field $\mathbf{B}_0$. In ordinary resonance (with $\mathbf{B}_0 = 0$), the obliquely incident P-polarized component (with the wave electric field in the plane of incidence) has an electric field oscillation along the density gradient. In magnetic resonance, occurring even at normal incidence, the transverse electric field oscillates normal to the density gradient but the $\mathbf{V}_{os} \times \mathbf{B}_0$ force induces electron oscillations along the density gradient. In either case these oscillations along the density gradient produce charge separation and drive plasma waves. The transverse waves propagate up to the appropriate cutoff density and tunnel in to drive waves at the resonant density, which are then damped into plasma energy. Langmuir waves are involved in ordinary resonance, and similarly for upper-hybrid waves in magnetic resonance. A large value of θ or B_0 implies a large transverse electric field at cutoff, while a small value of θ or B_0 implies a more efficient tunneling. There is thus an optimum θ or B_0 for energy transfer to the plasma.

There has been considerable theoretical work on resonant absorption. Thomson, Max & Estabrook (1975) made the first calculation of magnetic field generation by resonant absorption. Nishihara & Ohsawa (1976) pointed out the role of thermal motion. Utilizing the nonlinear current, Bezzerides *et al.* (1977) calculated the saturated ($S^r = 0$) magnetic field and found that it was confined to a narrow region around resonance. However, Woo & DeGroot (1978b) and Aliev & Bychenko (1981) showed that, owing to the inclusion of another term in the nonlinear current, the magnetic fields of resonant absorption would actually penetrate well into the overdense region. They could thus have an important effect on thermal transport. Aliev & Bychenko (1981) also showed that magnetic field generation was suppressed by plasma flow and by the already generated magnetic field. On the other

hand, Stefan & Frolov (1982) showed that density profile steepening causes a significant enhancement of the magnetic field.

The magnetic fields, once generated, can also have a pronounced effect on resonant absorption. An analytic, warm-plasma theory with a linear profile (Grebogi, Liu & Tripathi 1977) predicted a 70% absorption for normal incidence. An analytic and numerical study for oblique incidence in a magnetized plasma showed that there is an optimum combination of θ and B_0 and predicted that it is possible to obtain 99% absorption (Woo, Estabrook & DeGroot 1978).

4.4 *Field momentum deposition*

Two situations are considered briefly in this subsection for which a large magnetic field generation rate is expected owing to laser field momentum deposition. These are the high-irradiance experiments and laser filamentation. In these cases the field $\epsilon_i \omega g/ne$ has a large solenoidal component on account of the large radial variation of the laser intensity.

Consider first the magnetic field generation in a high-irradiance experiment. We assume a normally incident laser beam and take a right-handed cylindrical coordinate system (r, ϕ, z) with $I = -I_0\hat{z} \exp(-r^2/a^2)$. Then equation (12) shows that S_g^r is in an azimuthal direction $(+\hat{\phi})$ opposite the thermally generated fields and has a maximum $\left(\text{at } r = a/\sqrt{2}\right)$ magnitude in MG/ns of $6 \times 10^{-27} \nu(\text{s}^{-1})I_0(\text{W/cm}^2)/a(\text{microns})$. Thus, for collisional absorption $[\nu \sim 0\,(10^{12}\,\text{s}^{-1})]$, generation rates of a few MG/ns are expected for typical irradiances (10^{16} W/cm^2) and focal radii (15 microns). The rate could be even higher for turbulence-enhanced absorption (Mora & Pellat 1981b; Bychenkov *et al.* 1984). Since this field opposes the thermally generated field, it may explain the field reversal observed at Rutherford Laboratory (Raven, Willi & Rumsby 1978).

Because of the high laser intensity and very large radial variations (solenoidal character of forces), self-focused laser filaments are a natural place to expect magnetic field generation by radiative forces. In fact, Willi & Rumsby (1981) have observed magnetic fields surrounding self-focusing filaments. For sufficiently long filaments a quasi-steady axial condition can exist with the field momentum deposition force being balanced by the ordinary resistive drag force, i.e., momentum passing from laser fields to electrons to ions. The resulting current density is neV_d, where V_d/c is the ratio of the Poynting flux I to $n_{cr}mc^3$ (2.4×10^{18} W/cm^2 for a Nd–glass laser), independently of collision frequency. These magnetic fields, if dominant, can be experimentally distinguished from thermally generated fields by their opposite direction.

5. Measurements of spontaneous magnetic fields

Spontaneous magnetic fields have been studied with a variety of diagnostics. The earliest and most used method has been small induction coils placed near the target. Voltages, induced in the coil as the magnetic field structure expands past the coil, are recorded on an oscilloscope. A small, target-imbedded wire probe (Drouet & Bolton 1976) was also used to record directly the current flow through the target–plasma interface. More recently (Sakagami *et al.* 1979), the fields were recorded with audio-recording magnetic tape as the target material. These diagnostics all used physical probes that could not survive in the focal region of the laser but that responded to changes in nearby regions. However, optical methods (Faraday rotation and the Zeeman effect) do permit measurements in the laser–plasma interaction region — at the focus of the laser. These will be described after a brief discussion of measurements with physical probes.

5.1 *Measurements with physical probes*

The first measurement of a spontaneous magnetic field was in the laser-induced breakdown of a gas (Korobkin & Serov 1966) and was dependent on asymmetries in the focusing. The first magnetic fields observed for the laser irradiation of a solid target (Askar'yan *et al.* 1967) were attributed to currents produced by light pressure. There have been extensive theoretical studies (Section 4) of magnetic fields associated with laser radiation effects. However, for the lower irradiance used in this experiment the fields could have been due to thermal sources (Section 2.1) or (if in vacuum) to electron emission. Large (kilogauss) fields were measured when a laser beam was focused onto a solid target located in a low-pressure background gas (Stamper *et al.* 1971). The fields, which were observed to be azimuthal about the laser axis, were explained in terms of thermal sources. The dependence of the magnetic fields on the background was studied, and it was noted that some field generation occurred in the expanding front (Bird *et al.* 1973). The generation was affected by the ambient plasma, continuing after the laser probe and even reversing (McKee, Bird & Schwirzke 1974). A small early-time component was observed for a metallic target (Case & Schwirzke 1975) and explained in terms of thermionic electron emission during the laser probe. Schwirzke (1973) gave a good discussion of these magnetic probe studies. All of the studies discussed thus far used the induction probes.

Despite the involvement of the background, studies using a current probe (Drouet & Bolton 1976) were consistent with the field generation's being at the plasma–target interface. However, the current induced in a CO_2-laser plasma did show a resonance with background pressure (Drouet & Pepin 1976). Their studies also showed the role of photoionization and magnetic field diffusion (Drouet *et al.* 1976). The magnetic field expansion was later characterized by diffusion in the photoionized background followed by convection with the laser plasma (Drouet *et al.* 1977). Later induction probe studies (Edwards *et al.* 1977) also showed, as earlier (Case & Schwirzke 1975), that the magnetic field expanding from a metallic target has a fast component traveling with the front velocity. Probes with a subnanosecond response have shown that the rise of the magnetic field is synchronous with the initial formation of the plasma (Serov & Richardson 1976). A systematic magnetic probe study of the magnetic fields produced for a solid target in vacuum (Nakano & Sekiguchi 1979) was made and compared with a computer simulation. They found two distinctly different regions for the radial variation of the field and for the radial dependence of elasped time until maximum field. Studies (Sakagami *et al.* 1979; Sakagami, Kawakami & Yamanaka 1980), using audio magnetic tape as a target and as a magnetic field recording medium, have yielded the two-dimensional geometry of the fields and shown them to be consistent with resonant absorption.

5.2 *Optical measurements*

Although studies using physical probes have shown the magnetic field geometry, the involvement of the target in field generation, and the synchronicity of the rise with the laser probe, these probes are not able to sample directly the laser–plasma interaction region, i.e., in the focus of the laser. This is the region of field generation by thermal sources and the direct effects of laser radiation. Magnetic fields, up to a few megagauss in magnitude, have been measured in the laser focal region with the use of Faraday rotation and Zeeman profile diagnostics. These diagnostic techniques will be discussed here after a review of the results of these optical studies.

In the original Faraday rotation study (Stamper & Ripin 1975), planar solid targets were irradiated in vacuum with a tightly focused ($d \sim 35$ microns) 1.06-micron Nd-laser beam

at an irradiance of 10^{15} W/cm^2. Magnetic fields of several megagauss were observed by means of a Faraday rotation of a side-on second-harmonic (0.53-micron) probing laser and also of the specularly reflected main laser beam. Later measurements (Stamper, McLean & Ripin 1978; Raven, Willi & Rumsby 1978) used a Raman-shifted (0.633-micron) probing beam to avoid the difficulties of emitted second-harmonic light. Stamper, McLean & Ripin (1978) used a three-channel recording system and made measurements under a variety of experimental conditions (timing, target material and geometry, laser irradiance, polarization, and prepulse). All of the data were consistent with thermally generated magnetic fields in the standard ($\nabla T \times \nabla n$) direction. The fields were enhanced by a laser prepulse. Raven, Willi & Rumsby (1978), using, for the first time, simultaneous Faraday rotation and interferometry, were able to measure the magnetic field profiles. The profile, for an aluminum wire target at an irradiance of 10^{16} W/cm^2, showed a field maximum of 1.8 MG. The same data showed a reversed density gradient and possible field reversal near the target surface. Such conditions could result from the direct effects (ponderomotive steepening and field momentum deposition) of laser radiation.

Although magnetic fields had been observed (Stamper, McLean & Ripin 1978) for a tightly focused laser (25-micron) onto a large (120-micron) spherical target, they were not observed (Raven, Willi & Rumsby 1978) on small (45-micron) microballons. The dependence of the magnetic fields on target size and shape was investigated in another study (Raven *et al.* 1979). The field magnitude on spherical targets was dependent in the ratio *D/d* (of target to focal-spot diameter), with fields observable only for $D/d \geq 5$. This might be explained by the larger capacitance of larger stalk-supported targets, permitting more electron flow. Fields were also observed in the critical region ($n \sim 10^{21}$ cm^{-3}) of the main laser beam with a fourth-harmonic probe (0.26 micron). The special targets had a step discontinuity in *Z* (Tidman 1974). All of these studies had been conducted at an irradiance around 10^{16} W/cm^2. The most promising ICF pellet designs are now for an irradiance of 10^{14}–10^{15} W/cm^2 and with short-wavelength light. Willi, Rumsby & Duncan (1981) studied the effect of illumination uniformity for spherical targets in a lower-irradiance regime but with 1-micron light. They determined, for four-beam illumination, how the magnetic field decreased as the focal diameters and uniformity increased. No field greater than 100 kG was observed when the focal planes were farther from the target center than 4.5 target radii. This held up to the maximum obtainable irradiance of 4×10^{13} W/cm^2.

Faraday rotation has been used in the study of laser beam filamentation onto spherical targets (Willi, Rumsby & Duncan 1981). Magnetic fields as high as a few megagauss were observed surrounding the filaments. The authors proposed thermal sources ($\nabla T \times \nabla n$) or thermal instabilities (Tidman & Shanny 1974; Haines 1981) as explanations. However, as discussed in Section 4.4, if the intensity in the filament is sufficiently high, then laser field momentum deposition could account for the magnetic fields.

Faraday rotation of the backscattered 0.53-micron laser radiation (Briand *et al.* 1985) from a planar target was used to determine an axial magnetic field and thus to provide evidence for the dynamo effect (Section 3.5). A relative delay between the incident and backscattered beams permitted them, after they passed through separate polarizers, to be displayed side by side on a streak camera. The polarizations parallel and perpendicular to the incident polarization were spaced on opposite sides of the slit length. Data were taken with the back-scatter polarizer rotated at various small angles about the cross-polarized position of the (fixed) incident polarizer. A minimum in the perpendicular component of the backscatter signal occurred at an angle of 3° — the Faraday rotation angle. This gave an estimated axial magnetic field of 0.6 MG.

The Zeeman effect was used to measure magnetic fields for a 1-micron laser pulse onto a carbon target at an irradiance of 5×10^{12} W/cm^2 (McLean *et al.* 1984). The magnetic

field increased from 100 to 200 kG when the focal spot was changed from a flat-topped distribution to a ring pattern. This study is used as a basis for the discussion in Section 5.2.2 of the Zeeman profile diagnostic. A later Zeeman profile study (Briand *et al.* 1987) used a quarter-micron laser pulse onto a carbon target at an irradiance of 2×10^{14} W/cm^2. In this study the fluid-expansion Doppler shift permitted spatial resolution of the magnetic field and separation of the toroidal and axial fields. The maximum field observed (axial) was 0.5 MG.

5.2.1 *Faraday rotation diagnostic*

A plane-polarized electromagnetic wave propagating along a magnetic field remains plane polarized, but the plane of polarization rotates as the wave propagates along its path. The rate of change of the right-handed rotation angle ϕ with respect to distance z along the ray path is $d\phi/dz = (k_- - k_+)/2$, where the wave numbers (k_+ for the right-handed or positive helicity mode and k_- for the left-handed mode) are given by the usual dispersion relation for waves propagating along a magnetic field: $(ck_\pm/\omega)^2 = 1 - \omega_p^2/\omega(\omega \mp \omega_c)$. Thus the rotation angle depends on the path integral of density ($\omega_p^2 = \omega^2 n/n_{cr}$) times the magnetic field component along the path ($\omega_{cz} = eB_z/mc$). If $n\omega_{cz} \ll (n_{cr} - n)\omega$, then approximately $d\phi/dz = (\omega_p/\omega)^2(\omega_{cz}/2\bar{n}c)$, or

$$\phi(\text{deg}) = 1.51\lambda_p^2(\text{microns}) \int \frac{n(\text{cm}^{-3})B_z(\text{MG})\,dz\,(\text{microns})}{10^{21}\sqrt{1 - n/n_{cp}}}, \tag{13}$$

where $\bar{n} = \sqrt{1 - n/n_{cp}}$ is the refractive index, and λ_p and n_{cp} are the wavelength and the critical density for the probing beam.

With an independent determination of the density — via interferometry — one can unfold the integral to obtain the magnetic field. The rotation is right handed when $d\phi/dz > 0$, i.e., $k_- > k_+$. For Faraday rotation this means that the rotation is right or left handed according as the wave propagates parallel or antiparallel, respectively, to the magnetic field.

A plane-polarized, short-pulse probing laser beam is used for the Faraday rotation diagnostic. The probe beam is passed parallel to the target surface, and the probe light pattern in the target plane (which is normal to the probe beam axis) is imaged, after passing through a polarization analyzer, onto film. The Faraday rotation angle is obtained as a function of transverse (r–z) position in the target plane from the recorded intensity. This requires using the cosine-squared angular dependence of polarizer transmission and correcting for film response.

Now consider the light pattern that is expected when one looks through a tilted-polarization analyzer, with polarization axis An [left-hand side of figure 1(a)], at an oncoming vertically polarized ($\underline{E}_0$) probing laser beam that has passed out of the page through the thermally generated (azimuthal) magnetic field structure shown. Most of the background will be relatively dark owing to the almost-crossed polarizer. However, localized regions will be brighter or darker owing to Faraday rotation and thus signify the presence of magnetic fields. In regions (such as below the laser axis) where the probe beam propagates parallel to the magnetic field, the wave **E** vector is rotated to the left so that it is more nearly *cross polarized than the incident beam to the analyzer. However, in regions where the beam* propagates antiparallel to the magnetic field (such as above the laser axis), the **E** vector is rotated to the right and makes a smaller angle with the analyzer axis. This gives an enhanced transmission. Thus one would expect an up–down asymmetry — with a lighter region at the top than at the bottom.

Such a light pattern is observed experimentally (Stamper, McLean & Ripin 1978), as shown on the right in figure 1(a). A bright region is seen above the laser axis, and a dark-
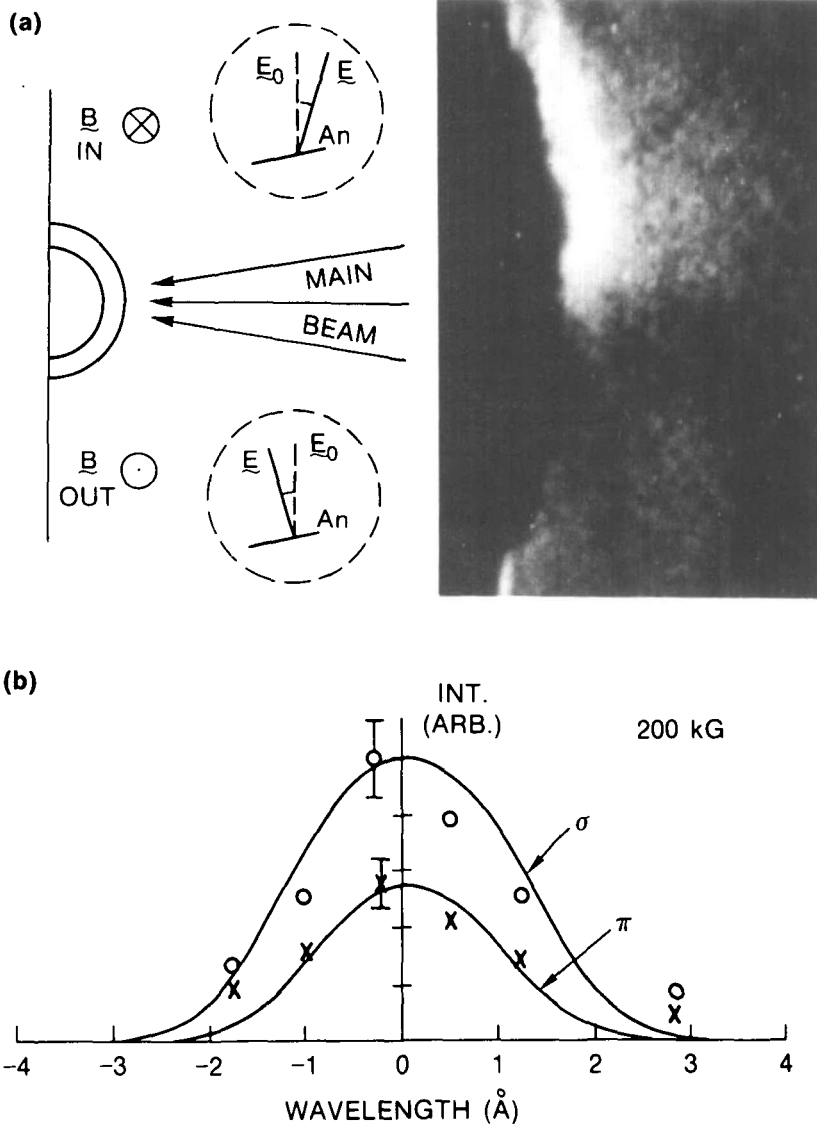
FIGURE 1. Optical data for spontaneous magnetic fields. (a) (Right) Faraday rotation light pattern. (Left) Azimuthal magnetic field and rotated **E** vectors (insets) that produced the pattern. (b) Zeeman profiles of the π and σ components, showing data (points) and calculated profiles (curves) for a 200-kG field.

ening (below background) is seen below the laser axis. The 75-ps (FWHM) main Nd–glass laser (1.05-micron) pulse, with a 3% prepulse, was incident from the right and was focused tightly (25 microns) onto a polystyrene $(CH_2)_n$ slab target to produce a high irradiance (10^{16} W/cm²). The peak of the 50-ps (FWHM) duration, nonharmonic (0.633-micron) probing laser pulse was 50 ps after the peak of the main laser probe. The polarizer was rotated 15° from the cross-polarized position. Because of the high irradiance and steep gradients, magnetic fields of a few megagauss were produced near the laser axis.

   In the experiments, where there are density gradient and magnetic field components

transverse to the propagation direction, there are polarization-dependent phase shifts that can cause some depolarization. When the propagation is normal to a density gradient, there is a phase shift between the S component (polarized normally to the gradient) and the P component (polarized parallel to the gradient), which can be expressed (Lehmberg & Stamper 1978) as the integral $(c/2\omega)\int \nabla^2(1/\bar{n})\,ds$ over the ray path. This S–P depolarization should be considered when, because of fast ($\sim f/1$) collectors or steep angles of incidence, there is strong refraction. The magnetic depolarization can be ignored for fields of a few megagauss.

5.2.2 *Zeeman profile diagnostic*

The discussion of this section, although based on a particular Zeeman study (McLean *et al.* 1984), illustrates general features of the diagnostic. Zeeman splitting of spectral lines in a magnetic field has the diagnostic advantages over Faraday rotation of being passive (not requiring a probing laser), giving an average magnetic field along the line of sight (without having an explicit dependence on density), and (when not limited by continuum radiation) allowing access to a higher-density region. The diagnostic does require, however, that other spectral broadening and shifting mechanisms (Doppler, Stark, instrumental), as well as opacity effects, be taken into account.

When the viewing is centered and perpendicular to the laser axis, light is observed (for a toroidal magnetic field) that is emitted perpendicularly to the field. It thus consists of two linearly polarized sets of components: the π components, polarized parallel to the magnetic field, and the σ components, polarized perpendicularly to the magnetic field. By recording both sets of components separately and simultaneously, one can utilize their characteristic differences to obtain a measurement of the magnetic field. The π components are grouped toward the center, while the σ components are grouped toward the wings of the multiplet. Thus absorption of the π profile is greater than absorption of the σ profile, so that the magnetic field changes the ratio of the intensities of the two profiles. Magnetic field effects can thus be observed even when differences in the optically thin line shapes are obscured by instrument broadening. In other words, opacity effects can enhance the sensitivity of the field measurement.

The helium-like C v $1s2s\,^3S_1$–$1s2p\,^3P_{2,1,0}$ multiplet ($J = 2$ at 2270.9 Å, $J = 1$ at 2279.9 Å, and $J = 0$ at 2277.3 Å) was chosen for the Zeeman diagnostic. This multiplet was chosen because it is in a convenient (quartz UV) spectral range, is insensitive to Stark broadening, and is emitted from a relatively hot (100-eV) region where large magnetic fields are expected. It should be noted that, for the magnetic fields of interest (0.1–1 MG), this multiplet is in the intermediate magnetic-field-strength regime and that the weak-field approximation cannot be used. An outline of the calculation, along with the resulting shifts and intensities, is given in the Appendix of the paper (McLean *et al.* 1984) on which this section is based.

In the experiment a pulsed Nd phosphate glass laser beam (30–40 J in 5 ns) at 1.05 micron irradiated a 50-micron-thick carbon foil target, for an irradiance of 5×10^{12} W/cm². The result is presented here for the interesting case of a ring-shaped laser focus (produced by the placement of a 7-cm-diameter mask ahead of the focusing lens), since this case illustrates how opacity effects can enhance the sensitivity of the magnetic field measurement. The interior of the plasma was cooler and denser than the surrounding ring, since the laser intensity was lower in the center. Light emitted perpendicularly to the laser axis, from a region centered 400 microns from the target surface, was collected and imaged onto the entrance slit of a spectrograph. A Wollaston prism, placed ahead of the entrance slit, was

oriented so that the two polarizations (σ and π) were separated to opposite ends of the slit. Since the entrance slit is imaged (inside the spectrograph) onto the exit slit, the σ and π emissions could be separately recorded (with photomultipliers) after the exit slit.

The resulting experimental data (points), along with the calculated profiles (curves), are shown in figure 1(b). The calculated profiles used a Stark–Doppler width of 0.6 Å, an instrumental width of 1.5 Å, opacity corrections, and a magnetic field of 200 kG. As explained above, the σ and π profiles have different intensities owing to opacity effects for their differing line shapes. The calculated profiles for 0 kG (other parameters fixed) were identical for the σ and π components. The analysis shows a magnetic field of 200 ± 75 kG.

6. Conclusion

A large amount of experimental and theoretical work on spontaneous magnetic fields has been discussed. The broad understanding that is developing is encouraging in view of the complexity of the problem. Laser-produced plasmas are difficult to characterize experimentally because of their small size, short duration, and large inhomogeneity. Numerical simulations of certain magnetic phenomena will need to be two or three dimensional and to contend with steep gradients. Nevertheless, experimental and theoretical work continues, and the computational and diagnostic capabilities are expanding rapidly. The prospects for a predictive understanding are encouraging.

Acknowledgment

REFERENCES

AFANASÉV, Y. V. *et al.* 1978 *Sov. Phys. JETP* **47**, 271.
ALIEV, Y. M. & BYCHENKO, V. Y. 1981 *Sov. J. Plasma Phys.* **7**, 55.
ALTERKOP, B. A. & MISHIN, E. V. 1974 *Phys. Lett. A* **46**, 319.
ALTERKOP, B. A., MISHIN, E. V. & RUKHADZE, A. A. 1974 *JETP Lett.* **19**, 170.
ASKAR'YAN, G. A. *et al.* 1967 *JETP Lett.* **5**, 93.
ATTWOOD, D. J. 1978 *IEEE J. Quantum Electron.* **QE-14**, 909.
AULUCK, S. K. H. 1986 *J. Plasma Phys.* **36**, 211.
BEZZERIDES, B. *et al.* 1977 *Phys. Rev. Lett.* **38**, 495.
BIRD, R. S. *et al.* 1973 *Phys. Rev. A* **7**, 1328.
BOL'SHOV, L. A., DREIZIN, Y. A. & DYKHNE, A. M. 1974 *JETP Lett.* **19**, 168.
BOL'SHOV, L. A. *et al.* 1979 *Sov. Phys. JETP* **50**, 1101.
BRAGINSKII, S. I. 1965 In *Reviews of Plasma Physics* (Consultants Bureau, New York), Vol. 1, p. 205.
BRIAND, J. *et al.* 1985 *Phys. Rev. Lett.* **54**, 38.
BRIAND, J. *et al.* 1987 *Phys. Fluids* **30**, 2893.
BROWNELL, J. H. 1979 *Comments Plasma Phys. Controlled Fusion* **4**, 131.
BYCHENKOV, V. Y., GRADOV, O. M. & CHOKPAROVA, G. A. 1984 *Sov. J. Plasma Phys.* **10**, 430.
CASE, R. S., JR. & SCHWIRZKE, F. 1975 *J. Appl. Phys.* **46**, 1493.
CHANDRASEKHAR, S. 1961 *Hydrodynamic and Hydromagnetic Stability* (Oxford University, Oxford), p. 466.
CHASE, J. B., LEBLANC, J. M. & WILSON, J. R. 1973 *Phys. Fluids* **16**, 1142.
COLOMBANT, D. G. & WINSOR, N. K. 1977 *Phys. Rev. Lett.* **38**, 697.
COLOMBANT, D. G. *et al.* 1975 *Phys. Fluids* **18**, 1687.

DAIDO, H. *et al.* 1986 *Phys. Rev. Lett.* **56**, 846.

DEGROOT, S. R. 1952 *Thermodynamics of Irreversible Processes* (North-Holland, Amsterdam), p. 159.

DRAGILA, R. 1987 *Phys. Fluids* **30**, 925.

DROUET, M. G. & BOLTON, R. 1976 *Phys. Rev. Lett.* **36**, 591.

DROUET, M. G. & PEPIN, H. 1976 *Appl. Phys. Lett.* **28**, 426.

DROUET, M. G. *et al.* 1976 *Appl. Phys. Lett.* **29**, 469.

DROUET, M. G. *et al.* 1977 *J. Appl. Phys.* **48**, 2525.

EDWARDS, D. F. *et al.* 1977 *Phys. Rev. A* **16**, 2437.

EMERY, M. H. 1984 Personal communication.

EMERY, M. H., GARDNER, J. H. & BORIS, J. P. 1985 In *10th International Conference in Plasma Physics and Controlled Nuclear Fusion Research, Vol. 3* (International Atomic Energy Agency, Vienna), p. 129.

EPPERLEIN, E. M. & HAINES, M. G. 1986 *Phys. Fluids* **29**, 1029.

ESTABROOK, K. 1978 *Phys. Rev. Lett.* **41**, 1808.

EVANS, R. G. 1986 *Plasma Phys. Controlled Fusion* **28**, 1021.

FORSLUND, D. W. & BRACKBILL, J. U. 1982 *Phys. Rev. Lett.* **48**, 1614.

GREBOGI, C., LIU, C. S. & TRIPATHI, V. K. 1977 *Phys. Rev. Lett.* **39**, 338.

HAINES, M. G. 1981 *Phys. Rev. Lett.* **47**, 917.

HAINES, M. G. 1986 *Can. J. Phys.* **64**, 912.

HASEGAWA, A. & MIMA, K. 1978 *Phys. Fluids* **21**, 87.

HASEGAWA, A. *et al.* 1986 *Phys. Rev. Lett.* **56**, 139.

HAUER, A. & MASON, R. J. 1983 *Phys. Rev. Lett.* **51**, 459.

HORA, H. 1981 *Physics of Laser Driven Plasmas* (Wiley, New York), Chaps. 8, 9.

JONES, R. D. 1983 *Phys. Rev. Lett.* **51**, 1269.

JONES, R. D. & MEAD, W. C. 1986 *Nucl. Fusion* **26**, 127.

KIEFFER, J. C. *et al.* 1983 *Phys. Rev. Lett.* **50**, 1054.

KITAGAWA, Y. *et al.* 1986 *Phys. Rev. Lett.* **56**, 2804.

KOROBKIN, V. V. & SEROV, R. V. 1966 *JETP Lett.* **4**, 70.

LEHMBERG, R. H. & STAMPER, J. A. 1978 *Phys. Fluids* **21**, 814.

MANHEIMER, W. 1977 *Phys. Fluids* **20**, 265.

MAX, C. E., MANHEIMER, W. M. & THOMSON, J. J. 1978 *Phys. Fluids* **21**, 128.

MCKEE, L. L., BIRD, R. S. & SCHWIRZKE, F. 1974 *Phys. Rev. A* **9**, 1305.

MCLEAN, E. A. *et al.* 1984 *Phys. Fluids* **27**, 1327.

MEAD, W. C. *et al.* 1976 *Phys. Rev. Lett.* **37**, 489.

MEAD, W. C. *et al.* 1984 *Phys. Fluids* **27**, 1301.

MIMA, K., TAJIMA, T. & LEBOEUF, J. N. 1978 *Phys. Rev. Lett.* **41**, 1715.

MORA, P. & PELLAT, R. 1979 *Phys. Fluids* **22**, 2408.

MORA, P. & PELLAT, R. 1981a *Phys. Fluids* **24**, 2219.

MORA, P. & PELLAT, R. 1981b *Phys. Fluids* **24**, 2227.

NAKANO, N. & SEKIGUCHI, T. 1979 *J. Phys. Soc. Jpn.* **46**, 960.

NISHIGUCHI, A. & YABE, T. 1983 ILE Quarterly Progress Report on Inertial Fusion Program, January–March 1983, No. 5, p. 17.

NISHIGUCHI, A. *et al.* 1984 *Phys. Rev. Lett.* **53**, 262.

NISHIHARA, A. & OHSAWA, Y. 1976 *Phys. Fluids* **19**, 1833.

NUCKOLLS, J. H. 1973 LLL Semiannual Report, July–December 1973, UCRL-50021-73-2, pp. 76–81.

PERT, G. J. 1977 *J. Plasma Phys.* **18**, 227.

RAVEN, A., WILLI, O. & RUMSBY, P. T. 1978 *Phys. Rev. Lett.* **41**, 554.

RAVEN, A. *et al.* 1979 *Appl. Phys. Lett.* **35**, 526.

RIPIN, B. H. *et al.* 1975 *Phys. Rev. Lett.* **34**, 1313.

SAKAGAMI, Y., KAWAKAMI, H. & YAMANAKA, C. 1980 *Phys. Rev. A* **21**, 882.

SAKAGAMI, Y. *et al.* 1979 *Phys. Rev. Lett.* **42**, 839.

SCHMIDT, G. 1979 *Phys. Lett. A* **74**, 222.

SCHWIRZKE, F. 1974 In *Laser Interaction and Related Plasma Phenomena*, H. Schwarz & H. Hora, eds. (Plenum, New York), Vol. 2, p. 273.

SEROV, R. & RICHARDSON, M. C. 1976 *Appl. Phys. Lett.* **28**, 115.

SHKAROFSKY, J. P. 1980 *Phys. Fluids* **23**, 52.

SPITZER, L., JR. 1962 *Physics of Fully Ionized Gases* (Interscience, New York), p. 26ff.

STAMPER, J. A. 1972 Naval Research Laboratory Report 7411.

STAMPER, J. A. 1976 *Phys. Fluids* **19**, 758.

STAMPER, J. A. 1977 In *Laser Interaction and Related Plasma Phenomena*, H. Schwarz & H. Hora, eds. (Plenum, New York), Vol. 4B, p. 721.

STAMPER, J. A. & BODNER, S. E. 1976 *Phys. Rev. Lett.* **37**, 435.

STAMPER, J. A. & RIPIN, B. H. 1975 *Phys. Rev. Lett.* **34**, 138.

STAMPER, J. A. & TIDMAN, D. A. 1973 *Phys. Fluids* **16**, 2024.

STAMPER, J. A., McLEAN, E. A. & RIPIN, B. H. 1978 *Phys. Rev. Lett.* **40**, 1177.

STAMPER, J. A. *et al.* 1971 *Phys. Rev. Lett.* **26**, 1012.

STEFAN, V. & FROLOV, A. A. 1982 *Phys. Lett. A* **87**, 398.

STEIGER, A. D. & WOODS, C. H. 1972 *Phys. Rev. A* **5**, 1467.

TERAI, K. *et al.* 1985 *Appl. Phys. Lett.* **46**, 355.

THOMSON, J. J., MAX, C. E. & ESTABROOK, K. 1975 *Phys. Rev. Lett.* **35**, 663.

TIDMAN, D. A. 1974 *Phys. Rev. Lett.* **32**, 1179.

TIDMAN, D. A. 1975 *Phys. Fluids* **18**, 1454.

TIDMAN, D. A. & SHANNY, R. A. 1974 *Phys. Fluids* **17**, 1207.

TIDMAN, D. A. & STAMPER, J. A. 1973 *Appl. Phys. Lett.* **22**, 498.

WIDNER, M. M. & WRIGHT, T. P. 1974 Personal communication.

WILLI, O. & RUMSBY, P. T. 1981 *Opt. Commun.* **37**, 45.

WILLI, O., RUMSBY, P. T. & DUNCAN, C. 1981 *Opt. Commun.* **37**, 40.

WINSOR, N. K. & TIDMAN, D. A. 1973 *Phys. Rev. Lett.* **31**, 1044.

WITALIS, E. A. 1974 In *Laser Interaction and Related Plasma Phenomena*, H. Schwarz & H. Hora, eds. (Plenum, New York), Vol. 3A, p. 237.

WOO, W. & DEGROOT, J. S. 1978a *Phys. Fluids* **21**, 124.

WOO, W. & DEGROOT, J. S. 1978b *Phys. Fluids* **21**, 2072.

WOO, W., ESTABROOK, K. & DEGROOT, J. S. 1978 *Phys. Rev. Lett.* **40**, 1094.

YABE, T. & NIU, K. 1976 *J. Phys. Soc. Jpn.* **40**, 1221.

YABE, T. *et al.* 1983 *Phys. Rev. Lett.* **51**, 1869.

YATES, M. A. *et al.* 1982 *Phys. Rev. Lett.* **49**, 1702.